CFD-BASED MODELING OF A COHESIVELY SEPARATING SOIL LAYER IN CONSIDERATION OF LOCAL SOIL DISTRIBUTION

***C. Golla[1], H. Köhler[2] and F. Rüdiger[1]**
[1*] Institute of Fluid Mechanics, Technische Universität Dresden, Germany, christian.golla@tu-dresden.de
[2] Institute of Natural Materials Technology, Technische Universität Dresden, Germany

ABSTRACT

Predicting the cleaning time required to remove a thin layer of soil is a challenging task and subject of current research. One approach to tackle this problem is the description of physical sub-problems and the subsequent synthesis of these models. In this paper, an existing model for adhesive detachment is extended for the prediction of the cleaning time of cohesively separating soil layers. For this, the measured pull-off forces were correlated to the local water mass fraction. The model is validated with cleaning experiments with starch in a fully developed channel flow. Furthermore, an inhomogeneous soil distribution and its effect on cleaning results like cleaning time and removal rate is investigated. It is shown that a consideration of the local soil distribution in the model leads to a significant improvement of the prediction of the cleaning behaviour.

INTRODUCTION

Cleaning is an omnipresent topic whose importance has increased in recent decades. The food processing industry is a field where cleaning and decontamination is of utmost importance in order to avoid cross-contamination at product changeover or fulfill growing hygienic standards [1]. Although cleaning raises high economic and ecological costs [2], dimensioning of cleaning processes is often done empirically [3]. Modeling the cleaning process and a systematic variation of cleaning parameters can be used to minimize these costs. Cleaning processes, however, are complex multiphase problems that cannot be simulated on industrial scale with a reasonable amount of computational effort.

A cost-efficient way to model cleaning processes is using a boundary condition cleaning model (BCCM). In a BCCM, the soil behavior is modeled as a boundary condition for a computational fluid dynamics (CFD) problem. The BCCM approach was first introduced by Joppa et al. [4]. The underlying concept is to differentiate between soils according to their cleaning mechanism, which in turn is determined by the specific combination of the factors soil, cleaning fluid and substrate. The distinction used in this work, described in [5], distinguishes between diffusive dissolution, cohesive separation, adhesive detachment and viscous shifting. These cleaning mechanisms are also confirmed by other authors e.g. Welchner and Kessler [6], Fryer et al. [7] and Bhagat et al. [8]. Within this work, cohesive separation is considered, which is characterized by the overcome of the cohesive tension in the soil and the successive removal of the soil layer. In case of small particles (e.g. in the order of single molecules) removed, the particle transport is similar to diffusive dissolution.

In the recent decades a lot of experimental and numerical research in terms of modeling of cleaning has been conducted. Early work, e.g. from Yeckel et al. [9] deals with the prediction of a shear driven flow in an oil layer. Fernandes et al. [10] later applied these approaches to predict the cleaning of viscoplastic soils under usage of impinging water jets. Joppa et al. [11] developed a BCCM for the diffusive dissolution of a starch layer and validated it with cleaning experiments in a channel flow and with an impinging jet. This BCCM was based on the modeling approach of Xin et al. [12], developed for the mass transfer of whey protein. In 2014, Wilson et al. [13] presented a first approach for the prediction of the cleaning of an adhesively detaching soil. This was done by balancing hydrodynamic loads and a soil specific resistance. Köhler et al. [14] later introduced a BCCM for the cleaning of an adhesively detaching soil in a channel flow. The model was recently validated by Golla et al. [15] in a channel flow with a sudden expansion with locally varying flow properties.

Scope of this work is to develop a model for a cohesively separating soil on basis of the BCCM of Köhler et al. [14]. The model is used to investigate the influence of the local soil mass distribution on the cleaning kinetics. For that, the same starch as in Joppa et al. [16] is used as model soil and water as cleaning fluid. Transferability to the industrial case

ISBN: 978-0-9984188-2-7; Published online www.heatexchanger-fouling.com

of cleaning with *e.g.* hot sodium hydroxide solutions is expected, as long as the cleaning mechanism does not differ. For the development of the model, it is necessary to describe the binding forces of the starch under consideration of its swelling behavior. Therefore, a micromanipulation measurement technique, similar to the technique used by Liu et al. [17] or Zhang et al. [18] is utilized.

MODELING OF COHESIVE SEPARATION

Overview and modeling as boundary condition

For modeling, the process of cohesive separation is divided into subprocesses that are shown in Fig. 1. In the first step, the loads applied from the flow on the soil are calculated to determine a comparative stress τ_{hyd}. This is done by evaluating CFD simulation results. Next, the swelling behavior is described to calculate the local water mass fraction ω_{f} in the soil. This is crucial, since the water mass fraction is assumed to be the quantity determining the cohesive binding forces. In the next step the cohesive binding forces are described as a function of the water mass fraction: $\tau_{\mathrm{coh}} = f(\omega_{\mathrm{f}})$. Finally, a failure criterion is defined, which compares the hydraulic load τ_{hyd} and the cohesive binding stress τ_{coh} to decide, which amount of soil is removed by the flow.

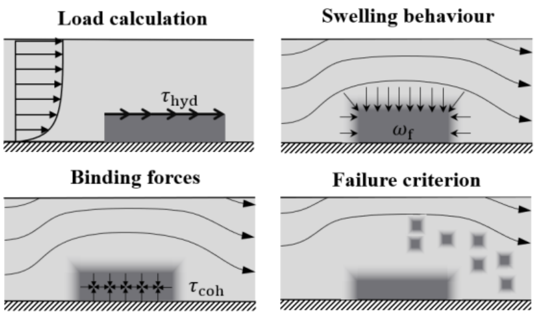

Fig.1: Division of cohesive separation in subprocesses for the modeling (similar to [14]).

The model is developed as a boundary condition for a CFD simulation. This is only permitted if the following assumptions hold [14]:

1. One way coupling between the fluid and the soil. This means that there are forces acting from the fluid on the soil but there is no feedback on the flow due to the swelling, or removal of the layer.
2. The height of the soil is negligible. Thus, the soil does not present an obstacle in the CFD simulation. There are just walls identified as soiled.
3. The swelling of the soil can be described with a one-dimensional diffusion equation with constant boundary conditions.

Modeling of the swelling kinetics

For the modeling of the swelling process a one-dimensional diffusion equation is used, since the thickness of the soil is small compared to the other dimensions. The diffusion equation reads:

$$\frac{\partial \omega_{\mathrm{f}}}{\partial t} = \frac{\partial}{\partial y}\left(D(\omega_{\mathrm{f}})\frac{\partial \omega_{\mathrm{f}}}{\partial y}\right). \qquad (1)$$

In Eq. (1), y is the wall-normal direction and D the diffusion coefficient. The latter, however, is not constant. Within this paper, two different approaches to model the swelling behavior are tested. On the one hand, the same power law approach $D = D_0 \omega_{\mathrm{f}}^{a}$ as used in [14] is tested. On the other hand, the exponential approach $D = D_0 e^{a\omega_{\mathrm{f}}}$, used in [16] to describe the swelling of starch, is tested. The boundary conditions for the swelling process are given as

$$\left.\frac{\partial \omega_{\mathrm{f}}}{\partial y}\right|_{y=0} = 0 \text{ and } \omega_{\mathrm{f}}(y = h_{\mathrm{s}}) = \omega_{\mathrm{max}}. \qquad (2)$$

On the bottom, at $y = 0$ the zero gradient condition represents the non-penetrable wall. On the top the maximum water mass fraction ω_{max} is assumed, which needs to be estimated experimentally. Due to the swelling, the height of the soil layer h_{s} is time dependent. The initial state refers to a dried soil with a constant initial water mass fraction ω_0.

The soil layer is discretized by means of finite volume method, using central differences for the spatial, and Euler forward for the temporal discretization. The procedure is described in detail in [19]. With the diffusion of the water into the soil, the height of the soil layer increases, which has influence on the diffusion process itself. This effect is taken into account by stretching the numerical grid. A detailed explanation of this technique is given in [14]. The numerical grid is shown in Fig. 2.

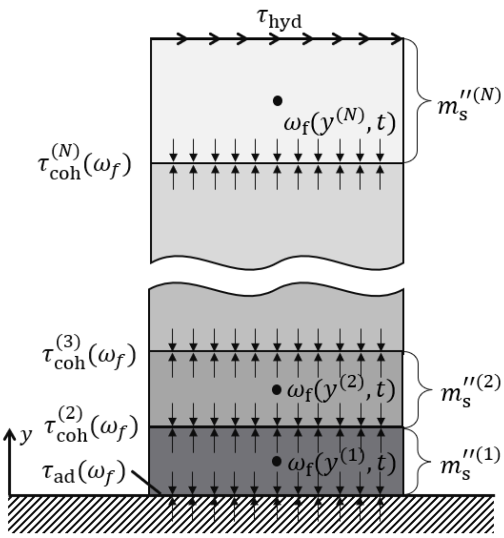

Fig.2: Sketch of the numerical discretization and the binding stresses.

Removal criterion and load calculation

Cohesive separation of a part of the soil layer occurs, once the hydrodynamic load overcomes the cohesive strength at some point within the soil. To model this, the cohesive strength needs to be determined experimentally and will be linked to the water mass fraction, calculated with the swelling model. In the finite volume framework, the water mass fraction is known at the cell centers. To decide whether a cell is removed or not, the cohesive binding forces must be described at the cell-to-cell interfaces. Thus, the water mass fraction is interpolated linearly. The location of the quantities is depicted in Fig. 2. Note that the bottom cell is in contact with the substrate. Thus, the removal of the last cell is adhesive detachment. Once these binding forces are described properly, the modeling approach inherently provides the opportunity to describe the change between the mechanisms cohesive separation and adhesive detachment. With that, the gradual removal of the cells can be described as follows:

$$m_{\mathrm{s}}'' = \sum_{i=1}^{N} m_{\mathrm{s}}''^{(i)}, \text{ with} \tag{3}$$

$$m_{\mathrm{s}}''^{(i)} = \begin{cases} m_{\mathrm{s},0}''^{(i)} & \tau_{\mathrm{coh}}^{(i)} \geq C\tau_{\mathrm{hyd}} \\ 0 & \tau_{\mathrm{coh}}^{(i)} < C\tau_{\mathrm{hyd}} \end{cases} \quad \text{and} \tag{4}$$

$$\tau_{\mathrm{coh}}^{(1)} = \tau_{\mathrm{ad}}. \tag{5}$$

The mass of cell i is denoted by $m_{\mathrm{s},i}''$. Once a cell is removed, it is considered to be flooded with water, i.e., it contains the maximum water mass fraction afterwards. This is equal to moving down the upper boundary condition from Eq. (2) to the next cell.

Note, that Eq. (3) describes the development of the mass at the dried state and does not consider the mass increase due to swelling. All results shown within this paper are with respect to the dry mass of the soil. The hydrodynamic load τ_{hyd} is determined by means of CFD. Within this paper, only wall shear stress is taken into account, yielding equation:

$$\tau_{\mathrm{hyd}} = \frac{1}{A_{\mathrm{p}}} \int_{A_{\mathrm{p}}} \left\| \underline{\underline{\tau}} \cdot \underline{n} \right\| \mathrm{d}A. \tag{6}$$

In Eq. (6) the magnitude of the wall shear stress is averaged across the soil surface A_{p}. The integral is evaluated numerically using the midpoint rule.

Equation (4) also includes a correction factor C. This is necessary to overcome the differences in the load application in the micromanipulation experiment and the fluid flow. It was first introduced in the original work from Köhler et al. [14]. Hooper et al. [20] also reported that the measured binding forces heavily depend on the load application.

Flow simulation and computational algorithm

All fluid flow simulations are carried out using the OpenFOAM CFD library, running the pimpleFoam solver. The governing equations for the problem are the incompressible Navier-Stokes-Equations which can be found in Ferziger et al [19]. For the turbulence modeling, a Reynolds averaged Navier Stokes (RANS)-framework is used. More precisely, a k-ω-SST turbulence model with a low Reynolds number adaption by Menter et al. [21] is utilized. The setup is a two-dimensional channel flow (cross section: 78 mm × 5 mm) with a given mean bulk velocity u_{b} between 0.5 and 3.0 m/s, which is described in detail in [4]. The resulting Reynolds numbers $Re = u_b D_h / \nu$ range from 5000 to 30,000. Once the CFD simulation is carried out, the averaged flow field is used to conduct the cleaning simulation. Within the cleaning simulation, the flow field remains unchanged. The soil behavior is implemented as a boundary condition, following the algorithm below in each time step.

1. Computation of the water mass fraction distribution in the soil layer, using Eq. (1) and (2).
2. Stretching of the numerical grid to consider the swelling of the soil layer.
3. Interpolation of the water mass fraction to the cell-to-cell interfaces and calculation of the cohesive binding forces.
4. Comparison of the cohesive binding forces with the hydrodynamic load, calculated from Eq. (6) and evaluation the removal criterion Eq. (3-5).

Modeling local soil distribution

In the simulation, only a single value for the initial soil mass coverage can be given. In reality, however, the soil mass coverage is randomly distributed. To consider this effect in the numerical modeling, a normal distribution of the soil is assumed with a mean value μ and a standard deviation σ. The density function of the normal distribution reads:

$$\varphi(z) = \frac{1}{\sqrt{2\pi\sigma^2}} e^{-\frac{(z-\mu)^2}{2\sigma^2}}. \tag{7}$$

The parameters μ and σ are determined by evaluating the experiments. To investigate the effect of the local soil distribution within the model, the simulation is run with different initial soil mass coverages in the range: $S = [\mu - 3\sigma, \mu + 3\sigma]$. This ensures, that 99.73 % of all possible outcomes are considered. It turns out, that an increment of $1\ \mathrm{g/m^2}$ for the simulation of the range described by S provides a sufficient resolution. After obtaining $m_s''(t)$ for different initial soil mass coverages $m_{s,0}''$, the weighted average with respect to the normal distribution is computed as

$$m_s''(t) = \sum_{m_{s,0}'' \in S} \varphi(m_{s,0}'') \cdot m_s''(t, m_{s,0}''). \tag{8}$$

MATERIALS AND METHODS

Soiling procedure and water mass fraction

For parametrization and validation of the cleaning model, precleaned stainless steel coupons (AISI 304, cold-rolled 2B finish) were soiled exactly as described in [4,5,11,16]. Starch (pre-gelatinized waxy maize starch, C Gel – Instant 12410, Cargill Deutschland GmbH, 150 g/l) was mixed with fluorescent zinc sulphide tracer crystals (4 g/l) in deionized water (30 °C) under stirring. The solution was sprayed on the test sheets and subsequently dried in a climate chamber (temperature of 23 °C, relative humidity of 50 %) for about 20 hours. The resulting surface soil mass coverage $m''_{\mathrm{s},0}$ was determined by differential weighing.

The initial water mass fraction ω_0 of the dried samples was determined by measuring the dry matter using the gravimetric method. Three samples were dried at 103 °C for several hours until mass constancy was achieved. By assuming that water is the only fraction that evaporates, the water mass fraction was calculated with $\omega_0 = 0.138 \pm 0.013$.

Unsteady soil layer thickness measurements

Measurements of the unsteady soil layer growth due to swelling were performed similar to [14]. Soiled test samples with different $m''_{\mathrm{s},0}$ were immersed in water at 23 °C. The samples were placed horizontally in a transparent basin. With the aid of a camera whose optical axis was aligned parallel to and within the substrate surface, a diffuse light source from behind, and a threshold-based image analysis procedure, the change in soil layer thickness was measured.

Micromanipulation measurements

The determination of the binding forces was conducted with a micromanipulation device as described in [14]. A soiled sample was immersed in water at 23 °C for a predefined soaking time of $t_{\mathrm{soak}} = 45$ s. Subsequently, the sample was lifted out of the bath and a scraper blade pulled off parts of the soil layer at a predefined gap δ_{gap} which was adjusted between the substrate surface and the bottom tip of the scraper blade. During this process, the force was measured with a sensor (KD40s 2 N, ME-Meßsysteme GmbH) directly coupled to the blade. An average force $\bar{F}$ is calculated as a scalar result while the scraper blade is between the beginning and the end of the sample.

Cleaning experiments and evaluation procedure

Test samples with $m''_{\mathrm{s},0}$ in the range of 30 g/m² to 80 g/m² were cleaned in a test rig with a fully developed turbulent flow of deionized water at (25 ± 1) °C flowing through a plane channel (cross section: 78 mm × 5 mm) at a given mean bulk velocity u_{b} of 0.5, 1.0, 2.0 or 3.0 m/s. The test rig is described and depicted in [4]. In total 41 valid experiments were conducted.

One side of the channel is soiled and the opposite side is transparent to measure the local cleaning progress with a gray scale camera in terms of the local intensity $\mathrm{I}_{\mathrm{raw}}$. An exemplary image sequence and the data evaluation procedure are presented in [5]. The evaluation modification as described in [14] was here also applied: a centered 40 mm × 40 mm large area of a sample was subdivided into 1 mm × 1 mm large subareas, wherein an average was taken over about 36 pixels. The initial local grey value $I_{\mathrm{raw},0}$ and a previously determined calibration [5] was used to calculate the local initial soil mass distribution. Subsequently an increase in the grey value is observed which occurs due to the swelling of starch. This can be corrected by using a swelling correction, employed in [11]. With that, the local cleaning time $t_{\mathrm{c},90}$, where 10 % of the initial soil mass remains, was determined. The mean 90 % cleaning time $\bar{\bar{t}}_{\mathrm{c},90}$ and its standard deviation were finally calculated over all subareas.

RESULTS

Model parametrization

Swelling kinetics and binding forces

Figure 3 shows the results of the soil layer thickness measurements. The pattern for all investigated soil mass coverages is similar: At the beginning, there is a steep increase, followed by an asymptotic approach to a saturation value. The investigated height ratio is $r_h = h_{\max}/h_0 = 10.72 \pm 0.46$. The qualitative swelling behavior is similar to dried ketchup, observed by Köhler et al. [14], although the height ratio is found to be three times higher. Assuming the amount of starch in the soil stays the same, the maximum water mass fraction is determined according to Köhler et al. [14] to $\omega_{\max} = 0.91$.

The thickness measurements are used to estimate the diffusion parameters D_0 and a in Eq. (1). This is done by a systematic variation of the parameters and evaluation of the root-mean-square-error (RSME). The best results are obtained for an exponential diffusion coefficient $D(\omega_{\mathrm{f}}) = D_0 e^{a\omega_{\mathrm{f}}}$ with the parameters $D_0 = 0.5 \cdot 10^{-9}\ \mathrm{m}^2/\mathrm{s}$ and $a = 2.06$. The numerical results with this model are shown in Fig. 3, termed as *model best fit*. Note that a second model is shown in the diagram, which will be motivated in the next paragraph.

To determine the binding forces, measurements with varying δ_{gap} were conducted, using two different initial soil mass coverages: 50 and 70 $\mathrm{g/m}^2$ respectively. The results are shown in Fig. 4, where the forces, normalized with the sample width $B = 20$ mm, are plotted over the penetration height h_{pen}. The penetration height, however, is not given a priori and is estimated using the swelling experiments (Fig. 3) by interpolating the value of the soil layer thickness h_s for the given wetting time. The penetration height is calculated as:

$$h_{\text{pen}} = h_s\left(m''_{\text{s},0}, t_{\text{soak}}\right) - \delta_{\text{gap}}. \tag{10}$$

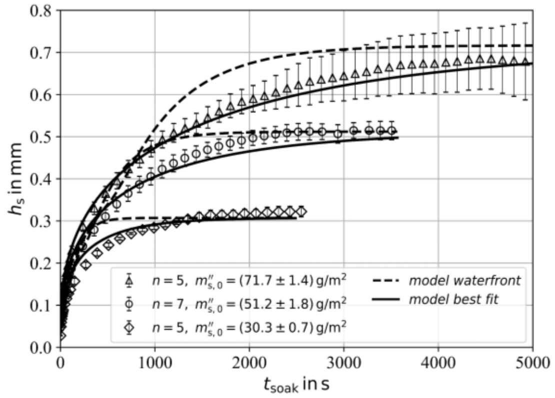

Fig. 3: Swelling kinetics measured for different initial soil mass coverages compared to the numerical modeling results.

First, it can be seen, that the pull-off forces increase exponentially with the penetration height. Second, the forces measured do not depend on the initial soil mass coverages. This indicates that a waterfront is propagating through the soil layer and after 45 s, the waterfront has not reached the substrate so that the measured forces are independent of the initial thickness of the soil layer.

In the consecutive step, the measured pull-off forces are used to describe the cohesive binding forces. However, the measured pull-off forces are composed of the force necessary to deform the layer in front of the blade, the force required to move up the material and the actual cohesive binding forces [22]. Since there is no valid approach in the literature to separate these shares, the measured force is assumed to be the cohesive binding force, knowing, that this leads to a systematic error. It is assumed that the correction factor in Eq. (4) can also be used to compensate this effect. For the modeling, the forces are normalized with the area of the sample to obtain a comparative stress τ_{coh}. This is also shown in Fig. 4.

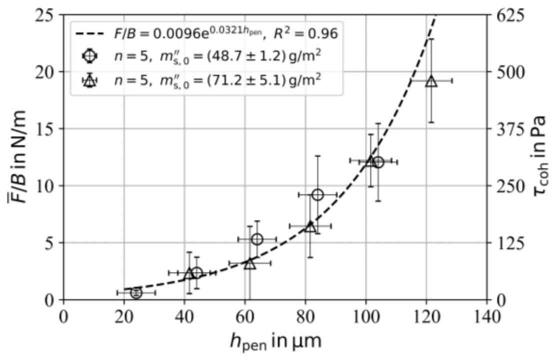

Fig.4: Measured averaged pull-off forces $\bar{F}$, normalized with the sample width B (left axis) and the sample area $B \cdot L$ (right axis).

In Fig. 5, left, the cohesive stress τ_{coh} is plotted against the water mass fraction at the tip of the scraper blade $\omega_{\text{f}}(t = t_{\text{wet}},\ y = \delta_{\text{gap}})$, which is determined using the *best fit* swelling model. It can be seen, that this procedure results in two different exponential functions $\tau_{coh} = f(\omega_{\text{f}}, m''_{\text{s},0})$, depending on the initial soil mass coverage. This is contrary to the observations made in Fig. 4. A possible explanation could be, that the swelling model *best fit* provides a reasonable prediction of the total water mass fraction within the whole soil layer, which is proven by the accordance with the measured soil layer thicknesses (Fig. 3). The model, however, fails to describe the water mass distribution across the soil properly. The literature also states that the diffusion behavior of some polymers cannot be described sufficiently by using Fick's law with constant boundary conditions, especially when extensive swelling of the polymers is caused [23]. The wetting of the polymer causes structural changes which can lead to internal stresses which results in non-Fickian diffusion processes [24].

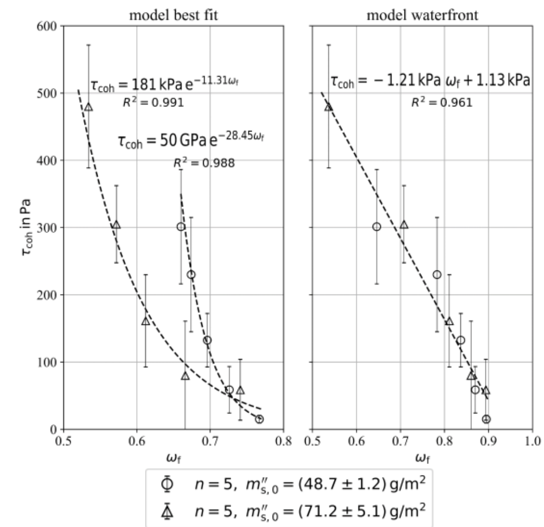

Fig. 5: Cohesive stresses related to the water mass fraction with the *model best fit* (left) and *model waterfront* (right).

One approach utilized to overcome this issue is to use extreme values for the diffusion model parameters D_0 and a to obtain the behavior of a waterfront propagating through the soil layer. Using a power-law approach $D(\omega_{\text{f}}) = D_0\omega_{\text{f}}^a$ with the parameters $D_0 = 0.75 \cdot 10^{-9}\ \text{m}^2/\text{s}$ and $a = 10$ leads to a swelling model with the described properties. This model is further termed as *model waterfront*. Figure 6 shows the difference between both models regarding the qualitative distribution of the water mass fraction over the penetration height.

Under usage of the *waterfront* model, the cohesive stress can be related to the water mass fraction, independent of the initial soil mass coverage. This is shown in Fig. 5, right.

The predicted swelling kinetics can also be compared to the soil thickness measurements (Fig. 3). The comparison, however, does not show a good agreement with the experiments. This indicates again that a more complex diffusion model, including e.g. non-Fickian diffusion, would be necessary to fully capture the swelling behavior of the starch.

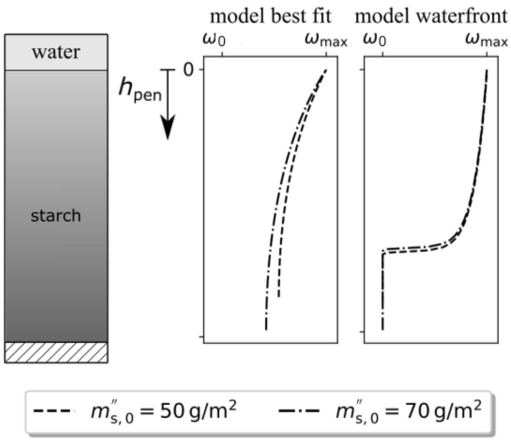

Fig. 6: Qualitative comparison between the *model best* fit and the *model waterfront* regarding the water mass distribution across the soil layer height.

In the rest of the paper both models are further evaluated in terms of feasibility to conduct cleaning simulations. For the model *best fit* the $\tau_{\mathrm{coh}}(\omega_{\mathrm{f}})$ determined for $m''_{\mathrm{s},0} = 50\ \mathrm{g/m^2}$ is utilized, since this is closer to the majority of the investigated soil mass coverages in the cleaning experiments.

Estimating the correction factor

Finally, the correction factor needs to be determined. Consequently, simulations under consideration of the soil mass coverage distribution were conducted and the results were adjusted to match the experimental data in terms of the 90% cleaning time $\bar{\bar{t}}_{\mathrm{c},90}$.

It was found that the correction factor is not independent from the flow velocity. It can be expressed in terms of the Reynolds number of the flow as follows:

$$C = C_0 Re^{-0.88}. \qquad (11)$$

In a plane turbulent channel flow, quantities often show a dependency from the Reynolds number to the power of 0.88. For instance the friction factor C_{f} can be expressed the same way [25].

The factor C_0 is finally estimated at single cleaning experiment using the simulation with a bulk velocity $u_{\mathrm{b}} = 1\ \mathrm{m/s}$ and an initial soil mass coverage $m''_{\mathrm{s},0} = (50 \pm 5)\ \mathrm{g/m^2}$. The values found are $C_0 = 356.64$ for the *model best fit* and $C_0 = 31974$ for the *model waterfront*.

Influence of the soil mass distribution

The cleaning experiments are evaluated with respect to the distribution of the initial soil mass coverage $m''_{\mathrm{s},0}$. Figure 7 shows the distribution of the soil mass coverage of a sample, whereby significant bright spots are attributed to tracer agglomerates.

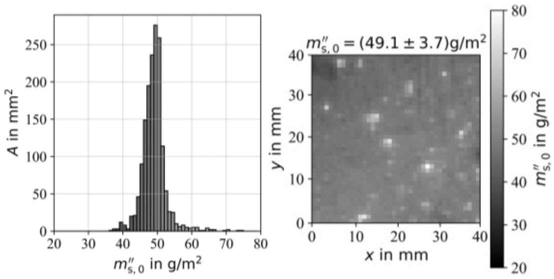

Fig. 7: Distribution of the initial soil mass coverage of a sample.

In the next step, the initial soil mass coverage of all the experiments is evaluated regarding the mean value μ and the standard deviation σ. The result is shown in Fig. 8.

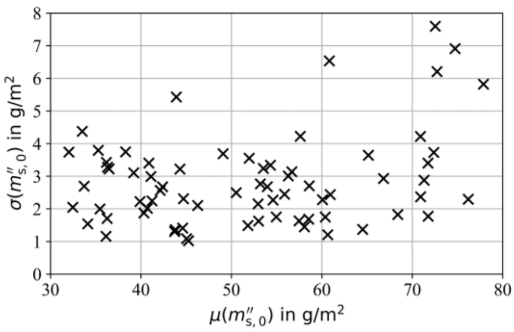

Fig. 8: Standard deviation σ of the initial soil mass distribution $m''_{\mathrm{s},0}$ over the mean value μ in the cleaning experiments

The evaluation shows no dependency of the standard deviation of the initial soil mass distribution from the mean value. However, for mean values greater than $60\ \mathrm{g/m^2}$, some larger standard deviations are observed. From Fig. 8 it can be seen that a value of $5\ \mathrm{g/m^2}$ provides a reasonable upper bound for the standard deviation. Hence, this value will be utilized as standard deviation in all simulations.

Using the determined information about the initial soil mass distribution, the simulations are conducted and the influence of the distribution on the course of soil mass coverage over time is evaluated. Figure 9 shows the dry soil mass coverage m''_{s} over time for the simulations with and without consideration of the distribution. A mean value of $50\ \mathrm{g/m^2}$ is investigated at a bulk velocity of $u_b = 1\ \mathrm{m/s}$. An experimental result is also shown for comparison. Note that the initial soil mass coverage of the experiment is slightly larger than in the simulation.

In the experiment, the cleaning starts after roughly 40 s with a constant removal rate. Below $10\ \mathrm{g/m^2}$ the removal rate decays. In the simulation the start of the cleaning is not predicted correctly both with consideration of the soil mass distribution and without. Although both models detect a removal of the first layer after 30 s (*model waterfront*) and 70 s (*model best fit*). The cleaning appears to be slower than observed in the experiment until $t \approx 200$ s. At this point, the consideration of the soil mass distribution becomes important: while in the simulation without considering the standard deviation the cleaning rate increases until total cleaning is observed, the cleaning rate remains constant in the simulations with consideration of the standard deviation. Below $10\ \mathrm{g/m^2}$ the removal rate decays as it was noticed in the experiments. Thus, the qualitative behavior of the simulations with consideration of the soil mass coverage distribution matches the experiments, although the cleaning at the beginning is predicted to slow and the removal rate in the middle of the process is overestimated. Both the *model best fit* and the *model waterfront* show a similar performance on the investigated case.

Note that the removal of the last remaining soil layer on the substrate only can be simulated properly when the information regarding the adhesion at the soil-substrate-interface is given. This is not investigated within this work.

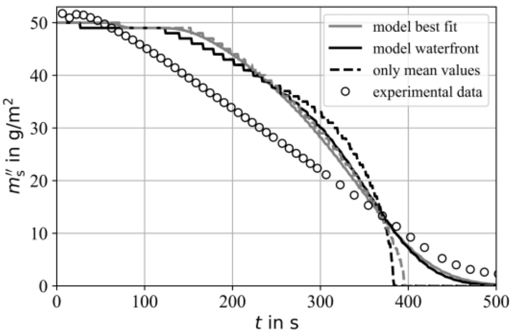

Fig. 9: Comparison of the course of soil mass coverage over time between simulations and experiments at $u_b = 1.0\ \mathrm{m/s}$ and $m''_{s,0} \approx 50\ \mathrm{g/m^2}$. The simulations are conducted with the models *best fit* and *waterfront*, both, with (solid lines) and without (dashed lines) consideration of the soil mass distribution.

Variation of soil mass coverage and bulk velocity

Evaluation of 90 % cleaning time

The influence of the soil mass coverage and the bulk velocity on the 90 % cleaning time is investigated in Fig. 10. Simulations were carried out at bulk velocities of $u_\mathrm{b} = (0.5, 1.0, 2.0, 3.0)\ \mathrm{m/s}$ with initial soil mass coverages of $m''_{s,0} = (30, 50, 70)\ \mathrm{g/m^2}$ with both models. For the standard deviation of the initial soil mass coverage a value of $5\ \mathrm{g/m^2}$ was used.

In the experiments the cleaning time increases with the initial soil mass coverage. From the experiments at $1.0\ \mathrm{m/s}$ and $2.0\ \mathrm{m/s}$ the conclusion can be drawn, that the 90 % cleaning time increases linearly with the initial soil mass coverage. However, this is uncertain due to scattering of the experiments. At a soil mass coverage of $40\ \mathrm{g/m^2}$ the 90 % cleaning time decreases approximately linearly with increasing bulk velocity.

The simulations predict a linear dependency of the 90 % cleaning time from the initial soil mass coverages. For almost all cases shown, the predicted values are within the scattering of the experiments. However, for $u_b = 3.0\ \mathrm{m/s}$ the simulations underestimate the times. A reason for that could be that it took roughly 40 s in the experiments until the pump reached the target value for the flow velocity, whereas the simulation assumes a developed flow at all times. The simulated 90% cleaning times increase slightly faster than linear with the bulk velocity. Both models provide similar results.

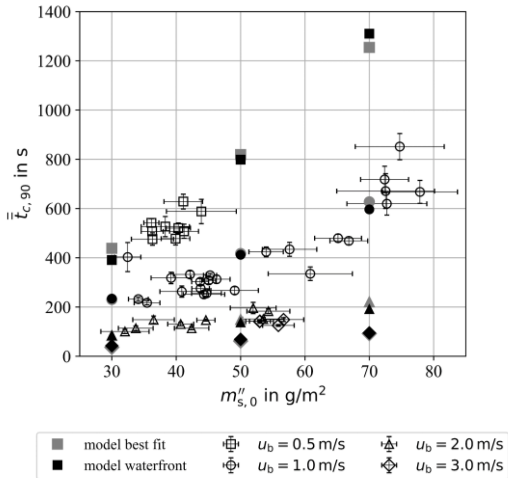

Fig. 10: Experimental and simulative results for the 90 % cleaning time for different bulk velocities and soil mass coverages. Error bars indicate standard deviations within each cleaning experiment.

Influence of soil mass coverage on cleaning rate

Three different initial soil mass coverages are further investigated regarding the cleaning rate, keeping the bulk velocity constant at $u_b = 1\ \mathrm{m/s}$. The results are shown in Fig. 11. Note that the experimental values for the initial soil mass coverage differ slightly from the simulative ones.

In the experiments, the cleaning rate is nearly independent of the initial soil mass coverage. This underlines the hypothesis that the cleaning time increases linearly with the initial soil mass coverage. The modeled cleaning rates are also nearly independent of the soil mass coverage. The predicted cleaning rates, however, are significantly larger than in the experiments. The beginning of the cleaning on the other hand is predicted to late, so that these effects compensate, and the predicted 90 % cleaning times show a decent agreement. The experiments also show that the start of the removal is delayed with increasing cleaning time. This effect is also represented in the simulations, although it is overestimated. Both models perform in a similar way. The *model waterfront*, however, shows slightly better agreement with the experiments.

Influence of bulk velocity on cleaning rate

Bulk velocities of $u_\mathrm{b} = 0.5, 1.0, 2.0, \mathrm{m/s}$ are investigated at an initial soil mass coverage of $m''_{\mathrm{s},0} = 40\ \mathrm{g/m^2}$, shown in Fig. 12. In the experiment, the observed cleaning rates increase approximately linearly with increasing bulk velocity. An increase of the cleaning rate with the bulk velocity is also observed in the simulations, although it is not linear. Aside from that, the simulations show the same discrepancies to the experiments as already discussed in the previous section. However, at $2.0\ \mathrm{m/s}$ the simulation shows a very good agreement with the experiment.

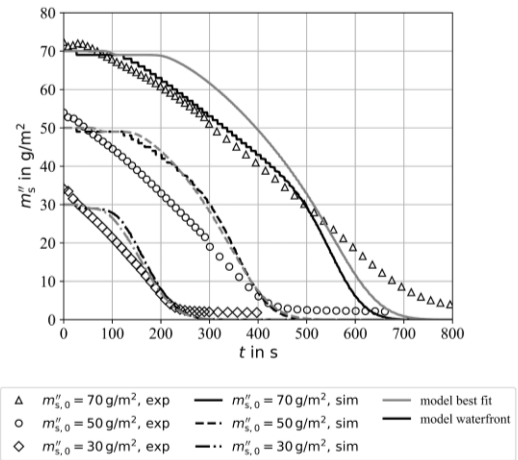

Fig. 11: Course of cleaning over time for different initial soil mass coverages $m''_{\mathrm{s},0}$ at a bulk velocity of $u_b = 1.0\ \mathrm{m/s}$.

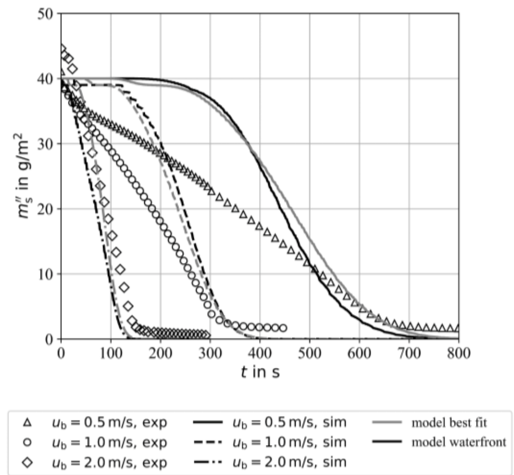

Fig. 12: Course of cleaning over time for different bulk velocities with an initial soil mass coverage of $m''_{\mathrm{s},0} = 40\ \mathrm{g/m^2}$.

CONCLUSION

In this paper, a BCCM for a cohesively separating soil layer was presented. The model was parameterized using bench scale experiments. Extensive investigations on the modeling of the cohesive binding forces and the influence of the soil mass distribution were presented. The model results were compared with experimental data.

The results of the investigation of the cohesive binding forces show, that a swelling model only considering Fickian diffusion is not sufficient to describe the swelling of starch. A workaround was created to represent some important swelling characteristics of starch. Furthermore, a methodology was developed, to take statistical fluctuations of the soil mass coverage into account. It was shown that considering the soil mass distribution in the simulation provides significantly better agreement between simulations and experiments. The presented model mainly shows a good qualitative agreement with the experiments. Although the values predicted for the 90 % cleaning times seems to match with the experiments, the model lacks in predicting the beginning of the removal and the cleaning rates properly, so that quantitative predictions should be viewed with caution.

In the future, the implementation of approaches considering non-Fickian diffusion should be considered. Also, further investigation of the cohesive binding forces could be promising to separate the single load components. The presented model also describes adhesive detachment inherently. Thus, the simulation of a transition between these cleaning mechanisms becomes feasible. When providing sufficient information about the binding forces, the model has the potential to get closer to the simulation of real industrial cleaning processes that involve changes in cleaning fluid and temperature.

ACKNOWLEDGEMENT

This research project is supported by the Industrievereinigung für Lebensmitteltechnologie und Verpackung e. V. (IVLV), the Arbeitsgemeinschaft industrieller Forschungs-vereinigungen “Otto von Guericke” e. V. (AiF) and the Federal Ministry of Economic Affairs and Climate Action (IGF 21334 BR). We thank Sebastian Kricke for performing the cleaning experiments, Dirk Oevermann for conducting swelling experiments and micromanipulation measurements, Sepp Höhne for preliminary studies on the presented model as well as Vera Liebmann for the critical revision of the manuscript.

NOMENCLATURE

Roman

a Diffusion parameter, $-$
A Area, $\mathrm{m^2}$
B Width of the sample, m
C Correction factor, $-$
D Diffusion coefficient, $\mathrm{m^2/s}$
D_0 Diffusion parameter, $\mathrm{m^2/s}$
D_h Hydraulic diameter, $D_\mathrm{h} = 4A/P$, m
$\bar{F}$ Averaged pull-off force, N
h Height, m
L Length of the sample, m
m Mass, kg
m'' Mass coverage, $\mathrm{kg/m^2}$
n Number of experiments, $-$
$\underline{n}$ Normal vector, m
N Number of cells, $-$
P Wetted Perimeter, m
r_h Height ratio, $\mathrm{m/m}$
Re Reynolds number, $Re = u_\mathrm{b}D_\mathrm{h}/\nu$, $-$
S Set, $-$
t Time, s
$\bar{\bar{t}}$ Time, averaged in region of interest, s
u Mean velocity, $\mathrm{m/s}$
x Coordinate, main flow direction, m
y Coordinate, wall normal direction, m
z Variable of the density function, $-$

Greek

δ Gap, m
μ Mean value, $-$
σ Standard deviation, $-$
ν Kinematic viscosity, $\mathrm{m^2/s}$
τ Shear Stress, Pa
$\underline{\underline{\tau}}$ Shear Stress Tensor, Pa
ω Mass fraction, $\mathrm{kg/kg}$

Sub- and superscript

ad Adhesion
b Bulk
c Cleaning
coh Cohesion
dry Dried state
f Fluid, water
gap Gap
hyd Hydrodynamic
(i) Index, $i = 1 \dots N$
max Maximum
p Patch
pen Penetration
raw Raw
s Soil
soak Soaking
0 Initial state
90 90%

REFERENCES

[1] Landel, J. R. and Wilson, D. I., The Fluid Mechanics of Cleaning and Decontamination of Surfaces, *Annual Reviews of Fluid Mechanics*, vol. 53, no. 1, pp. 147–171, 2021.

[2] Pettigrew, L., Blomenhofer, V., Hubert, S., Groß, F. and Delgado, A., Optimisation of water usage in a brewery clean-in-place system using reference nets, *Journal of Cleaner Production*, vol. 87, pp. 583–593, 2015.

[3] Tsai, J.-H., Huang, J.-Y. and Wilson, D. I., Life cycle assessment of cleaning-in-place operations in egg yolk powder production, *Journal of Cleaner Production*, vol. 278, pp. 123936, 2021.

[4] Joppa, M., Köhler, H., Rüdiger, F., Majschak, J.-P. and Fröhlich, J., Experiments and Simulations on the Cleaning of a Swellable Soil in Plane Channel Flow, *Heat Transfer Engineering*, vol. 38, no. 7–8, pp. 786–795, 2017.

[5] Köhler, H., Liebmann, V., Joppa, M., Fröhlich, J., Majschak, J.-P. and Fröhlich, J., On the concept of CFD-based prediction of cleaning for film-like soils, Proc. *13th International Conference on Heat Exchanger Fouling and Cleaning*, Warsaw, Poland, vol. 13, pp. 8-16, 2019.

[6] Welchner, K. and Kessler, H. G., Das Ausspülverhalten hochviskoser Produkte aus Rohrleitungen - Wechselwirkungen zwischen Produkt und Spülfluid, *Chemie Ingenieur Technik*, vol. 66, no. 9, pp. 1216–1217, 1994.

[7] Fryer, P. J., Robbins, P. T., Cole, P. M., Goode K. R., Zhang Z. and Asteriadou K., Populating the cleaning map: can data for cleaning be relevant across different lengthscales?, *Procedia Food Science*, vol. 1, pp. 1761–1767, 2011.

[8] Bhagat, R. K., Perera, A. M. and Wilson, D. I., Cleaning vessel walls by moving water jets: Simple models and supporting experiments, *Food Bioproducts Processing*, vol. 102, pp. 31–54, 2017.

[9] Yeckel, A., Strong, L. and Middleman, S., Viscous film flow in the stagnation region of the jet impinging on planar surface, *AIChE Journal*, vol. 40, no. 10, pp. 1611–1617, 1994.

[10] Fernandes, R. R., Tsai, J.-H. and Wilson, D. I., Comparison of models for predicting cleaning of viscoplastic soil layers by impinging coherent turbulent water jets, *Chemical Engineering Science*, vol. 248, pp. 117060, 2022.

[11] Joppa, M., Köhler, H., Kricke, S., Majschak, J.-P., Fröhlich, J. and Rüdiger, F., Simulation of jet cleaning: Diffusion model for swellable soils, *Food Bioproducts Processing*, vol. 113, p. 168–176, 2019.

[12] Xin, H., Chen, X. D. and Özkan, N., Removal of a model protein foulant from metal surfaces, *AIChE Journal*, vol. 50, no. 8, pp. 1961–1973, 2004.

[13] Wilson, D. I., Atkinson, P. Köhler, H., Mauermann, M., Stoye, H., Suddaby, K., Wang, T., Davidson and J. F., Majschak, J.-P., Cleaning of soft-solid soil layers on vertical and horizontal surfaces by stationary coherent impinging liquid jets, *Chemical Engineering Science*, vol. 109, p. 183–196, 2014.

[14] Köhler, H., Liebmann, V., Golla, C., Fröhlich, J. and Rüdiger F., Modeling and CFD-simulation of cleaning process for adhesively detaching film-like soils with respect to industrial application, *Food Bioproducts Processing*, vol. 129, pp. 157–167, 2021.

[15] Golla, C., Köhler, H., Liebmann, V., Fröhlich, J. and Rüdiger F., CFD-based Three-Dimensional Modeling of an Adhesively Detaching Soil Layer in a Channel Flow with Sudden Expansion, Proc. *Fouling and Cleaning in Food Processing 2022,* Lille, France, 2022.

[16] Joppa, M., Köhler, H., Rüdiger, F., Majschak, J.-P. and Fröhlich, J., Prediction of Cleaning by Means of Computational Fluid Dynamics: Implication of the Pre-wetting of a Swellable Soil, *Heat Transfer Engineering*, vol. 41, no. 2, pp. 178–188, 2020.

[17] Liu, W., Christian, G. K., Zhang, Z. and Fryer, P. J., Development and Use of a Micromanipulation Technique for Measuring the Force Required to Disrupt and Remove Fouling Deposits, *Food Bioproducts Processing*, vol. 80, no. 4, pp. 286–291, 2002.

[18] Zhang, Z., Ferenczi M. A., Lush, A. C. and Thomas, C. R., A novel micromanipulation technique for measuring the bursting strength of single mammalian cells, *Applied Microbiology Biotechnology*, vol. 36, no. 2, pp. 208–210, 1991.

[19] Ferziger, J. H., Peric, M. and Street, R. L., *Computational Methods for Fluid Dynamics,* 4th ed., Springer, 2020.

[20] Hooper, R. J., Liu, W., Fryer, P. J., Paterson, W. R., Wilson, D. I., and Zhang, Z., Comparative Studies of Fluid Dynamic Gauging and a Micromanipulation Probe for Strength Measurements, *Food Bioproducts Processing*, vol. 84, no. 4, pp. 353–358, 2006.

[21] Menter, F. R., Two-equation eddy-viscosity turbulence models for engineering applications, *AIAA Journal*, vol. 32, no. 8, pp. 1598–1605, 1994.

[22] Tsai, J.-H., Fernandes, R. R., and Wilson, D. I., Measurements and modelling of the 'millimanipulation' device to study the removal of soft solid layers from solid substrates, *Journal of Food Engineering*, vol. 285, pp. 110086, 2020.

[23] Crank, J., *The mathematics of diffusion*, 2nd ed. Clarendon Press, Oxford, 1975.

[24] Ferreira, J. A., Grassi, M., Gudiño, E. and de Oliveira, P., A new look to non-Fickian diffusion, *Applied Mathematical Modelling*, vol. 39, no. 1, pp. 194–204, 2015.

[25] Pope, S. B., *Turbulent Flows*, 1st ed. Cambridge University Press, 2000.

ISBN: 978-0-9984188-2-7; Published online www.heatexchanger-fouling.com